



Viscous flow past a collapsible channel as a model for self-excited oscillation of blood vessels



Chao Tang^a, Luoding Zhu^b, George Akingba^c, Xi-Yun Lu^{a,*}

^a Department of Modern Mechanics, University of Science and Technology of China, Hefei, Anhui 230026, China

^b Department of Mathematical Sciences, Indiana University-Purdue University, Indianapolis, 402 North Blackford Street, Indianapolis, IN 46202, USA

^c Division of Vascular Surgery, Department of Surgery, Indiana University-Purdue University, Indianapolis, IN 46202, USA

ARTICLE INFO

Article history:

Accepted 8 April 2015

Keywords:

Collapsible vessel
Blood-vessel interaction
Self-excited oscillation
Fluid–structure interaction
Wall shear stress

ABSTRACT

Motivated by collapse of blood vessels for both healthy and diseased situations under various circumstances in human body, we have performed computational studies on an incompressible viscous fluid past a rigid channel with part of its upper wall being replaced by a deformable beam. The Navier–Stokes equations governing the fluid flow are solved by a multi-block lattice Boltzmann method and the structural equation governing the elastic beam motion by a finite difference method. The mutual coupling of the fluid and solid is realized by the momentum exchange scheme. The present study focuses on the influences of the dimensionless parameters controlling the fluid–structure system on the collapse and self-excited oscillation of the beam and fluid dynamics downstream. The major conclusions obtained in this study are described as follows. The self-excited oscillation can be intrigued by application of an external pressure on the elastic portion of the channel and the part of the beam having the largest deformation tends to occur always towards the end portion of the deformable wall. The blood pressure and wall shear stress undergo significant variations near the portion of the greatest oscillation. The stretching motion has the most contribution to the total potential elastic energy of the oscillating beam.

© 2015 Elsevier Ltd. All rights reserved.

1. Introduction

Collapse and self-excited oscillation of blood vessels may occur to both healthy and diseased vessels. Coronary blood vessels may collapse when the heart contracts. Veins collapse in human legs in getting the blood pumped against the gravity towards the heart during physical exercise or physical therapy for deep-vein thrombosis (Dai et al., 1999). Harmful collapse and self-excited oscillation of the artery in arterial stenosis in patients with atherosclerosis could result in plaque rupture (Ku, 1997).

Our FSI model is motivated by the well known Starling resistor in which flow is driven through a thin-walled elastic tube mounted on two rigid tubes. The elastic tube is contained in a pressure chamber and the external pressure can be controlled to model the support of surrounding soft tissue of the blood vessel. Due to its rich dynamic behavior, some investigations have been made and reviewed by researchers (Grothberg and Jensen, 2004; Heil and Hazel, 2011). Experiments have found a rich variety of interesting phenomena, such as flow limitation, which is presented as the phenomenon that increasing the driving pressure of the flow does

not lead to a corresponding increase in the flow rate on the collapsed tube when the upstream transmural pressure is fixed, and a large number of different types of oscillations (Bertram et al., 1990; Wang et al., 2009). Most early theoretical analyses of flow in the Starling resistor were based on lumped-parameter or spatially 1D models (Cancelli and Pedley, 1985; Jensen, 1990), which involve a certain number of *ad hoc* assumptions and can be used to explain some behavior of collapsible tubes in early experiments. A closely related 2D physical model was introduced by Pedley (1992) first. Then 2D models in which the collapsible tube was simplified as a thin membrane (Luo and Pedley, 1996, 1998; Jensen and Heil, 2003) or an elastic beam (Luo et al., 2008; Liu et al., 2009) were widely used. Recent progress has been made on 3D models (Hazel and Heil, 2003; Marzo et al., 2005; Heil and Boyle, 2010). However, due to its complexity and high computing costs, 2D models are still being used to understand the rich dynamic behaviors of the system. It should be pointed out that in most of the existing works mentioned above, the membrane or beam is massless, i.e. the wall inertia is neglected. According to the previous research (Luo and Pedley, 1998; Bertram, 2008), when the dominant inertia resides in the wall, a typical flutter oscillation will occur, which is different from the classically observed collapsible-tube oscillation. In the present study, the elastic portion of the channel wall is modeled as

* Corresponding author.

E-mail address: xlu@ustc.edu.cn (X.-Y. Lu).

a massive beam and both stretching and bending modes of motion are considered.

2. Model problem and mathematical formulation

The model problem we consider is a two-dimensional viscous flow with density ρ and viscosity μ past a channel of width D . As shown in Fig. 1, a part of the upper wall of the channel is replaced by an elastic wall or beam. The remaining part of the channel walls is rigid. The upstream and downstream rigid portions of the upper wall have lengths of L_u and L_d , respectively. The initial position of the beam is a line segment joining point $(0, D)$ and point (L, D) . The Lagrangian coordinates for the two endpoints are $x_0 = 0$ and $x_0 = L$, respectively. The elastic beam has a length of L and is subjected to an external pressure p_e on its outer boundary. A steady Poiseuille flow for a Newtonian fluid is considered here and an average velocity U_0 is assumed at the inlet. A constant pressure p_d is specified at the outlet.

The incompressible Navier–Stokes equations are used to describe the flow dynamics and given as

$$\frac{\partial \mathbf{v}}{\partial t} + \mathbf{v} \cdot \nabla \mathbf{v} = -\frac{1}{\rho} \nabla p + \frac{\mu}{\rho} \nabla^2 \mathbf{v}, \tag{1}$$

$$\nabla \cdot \mathbf{v} = 0, \tag{2}$$

where \mathbf{v} is the velocity, p is the pressure, ρ is the density of the fluid and μ is the dynamic viscosity.

The structural equation governing the motion of the elastic beam is expressed in Lagrangian form

$$\rho_s \frac{\partial^2 \mathbf{X}}{\partial t^2} = \frac{\partial}{\partial s} \left[T(s) \frac{\partial \mathbf{X}}{\partial s} \right] - EI \frac{\partial^4 \mathbf{X}}{\partial s^4} + \mathbf{F}, \tag{3}$$

where s is the Lagrangian coordinate along the beam and \mathbf{X} is the position vector, ρ_s is the linear density of the beam, $T(s) = Eh((\partial \mathbf{X} / \partial s) - 1)$ is the tension with Eh the stretching rigidity, and EI is the bending rigidity. \mathbf{F} is the external force on the beam, i.e. force applied by the flow and the external pressure. The clamped condition is used at the two fixed ends,

$$\mathbf{X} = \mathbf{X}_0, \quad \frac{\partial \mathbf{X}}{\partial s} = (1, 0). \tag{4}$$

The reference quantities D , U_0 and ρ are chosen to non-dimensionalize the above mathematical formulation. Then, the present problem has five independent dimensionless parameters which are defined as

$$\begin{aligned} Re &= \frac{\rho U_0 D}{\mu}, & P_e &= \frac{P_e - P_d}{\rho U_0^2}, & M &= \frac{\rho_s}{\rho D}, & K_s &= \frac{Eh}{\rho U_0^2 D}, & K_b &= \frac{EI}{\rho U_0^2 D^3}, \end{aligned} \tag{5}$$

where Re is the Reynolds number, P_e is the external pressure on the beam, M is the mass ratio, K_s and K_b are the stretching and bending stiffness, respectively.

In the present study, the density ρ and the dynamic viscosity μ of the fluid are chosen as 1060 kg/m³ and 0.0035 kg/m/s. Moreover, the size of channel D is 5 mm and the average inlet velocity is 0.2–0.45 m/s to mimic the carotid artery. Thus the Reynolds

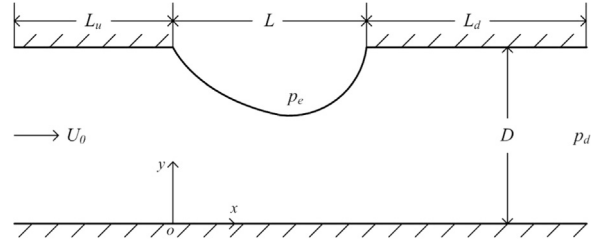


Fig. 1. Sketch of the flow-beam model (not to scale).

number ranges 300–650 approximately. In addition, according to our numerical examination with different computational domains, the domain is finally set as $L_u = 5D$, $L = 5D$ and $L_d = 30D$ unless otherwise stated. All of the quantitative results presented in this paper are in dimensionless form. Moreover, we fix $K_b/K_s = 10^{-5}$ in this study, which is the same as that used in the literature (Luo et al., 2008).

3. Numerical method

The fluid flow are solved numerically by the lattice Boltzmann method (LBM) (Chen and Doolen, 1998) which also handles the fluid and beam interaction in our problem. The lattice Boltzmann equation (LBE) with the multi-relaxation-time (MRT) model is

$$f_i(\mathbf{x} + \mathbf{e}_i \Delta t, t + \Delta t) - f_i(\mathbf{x}, t) = -S[f_i(\mathbf{x}, t) - f_i^{eq}(\mathbf{x}, t)], \tag{6}$$

where S is the collision matrix, Δt is the time increment, and $f_i(\mathbf{x}, t)$ is the distribution function for particles with velocity \mathbf{e}_i at position \mathbf{x} and time t . The equilibrium distribution function f_i^{eq} is defined as

$$f_i^{eq} = \omega_i \rho \left[1 + \frac{\mathbf{e}_i \cdot \mathbf{v}}{c_s} + \frac{\mathbf{v} \mathbf{v} : (\mathbf{e}_i \mathbf{e}_i - c_s^2 \mathbf{I})}{2c_s^4} \right], \tag{7}$$

where ω_i is the weighting factor, and c_s is the speed of sound. The velocity \mathbf{v} and density ρ can be obtained by the distribution functions

$$\rho = \sum_i f_i, \tag{8}$$

$$\rho \mathbf{v} = \sum_i \mathbf{e}_i f_i. \tag{9}$$

Here, we use the finite difference method to discrete the equation of the elastic beam. The detailed description of the algorithm has been given (Huang et al., 2007). The interaction of the fluid and the deformable beam is treated according to Buxton and Clarke (2006).

In addition, the relevant codes used for the present study have been also validated in our previous works. The numerical method has been applied with success to a wide range of cases such as viscous flow over a circular flexible plate (Hua et al., 2014), locomotion of a flapping flexible plate in a stationary fluid (Hua et al., 2013), hydrodynamic interaction of elastic filaments (Tian et al., 2011a), and viscous flow past three filaments in side-by-side arrangement (Tian et al., 2011b).

4. Results and discussion

4.1. Oscillation frequency and amplitude of the beam

We first investigate the effects of a variety of parameters on the oscillation frequency and amplitude of the elastic beam in self-excited oscillation. The parameters include the external pressure P_e ,

the Reynolds number Re , the stretching stiffness K_s , the mass ratio M , and the downstream length L_d . The excursion along both the x and y directions of the material point initially at the mid-point of the elastic beam is used as the oscillation amplitude of the beam.

Fig. 2(a) shows the oscillation frequency and amplitude of the beam versus the external pressure P_e . It is seen that both the frequency and amplitude increase with the increase of P_e . When P_e is relatively small, such as less than 4.0, the amplitude is less than 0.05 and the elastic beam behaves nearly steady. However, when P_e is greater than about 4.5, the amplitude increases significantly. This character indicates that the self-excited oscillation of the flexible beam can be triggered by an external pressure applied on the beam and the induced degree of oscillation enhances with the

increase of P_e . Furthermore, Fig. 2(b) shows the amplitude in the y -direction of the beam under the different external pressure P_e . The amplitudes increase with the increase of P_e , consistent with the preceding results. It is interesting to note that the maximum amplitude (i.e. the lowest point of the beam) always occurs around the position of $x=4.0$ for all the external pressures considered. This behavior is mainly related to both the external pressure and the inertia of the fluid flow exerted on the beam.

The trajectories of several typical points on the elastic beam in self-excited oscillation are plotted on Fig. 3. The four panels show the trajectories of four typical points with initial position at $x_0=1.0, 2.0, 3.0,$ and 4.0 , under the influence of different P_e . The trajectories are all closed curves, indicating that the oscillation of

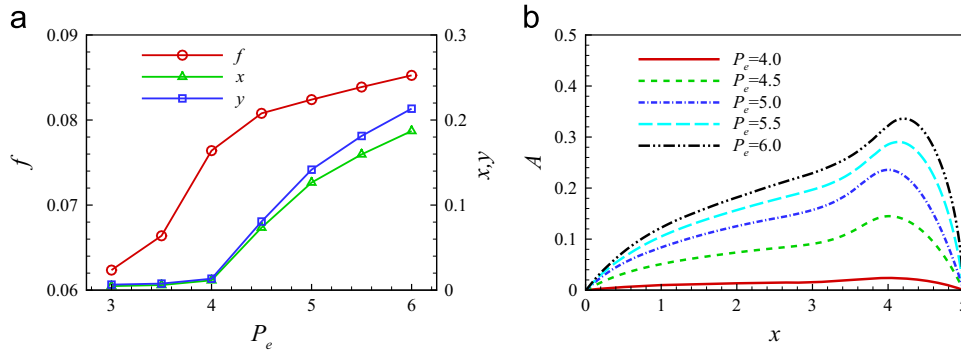


Fig. 2. Effects of the external pressure P_e on the oscillation frequency and amplitude with $Re=500, K_s=100,$ and $M=1$: (a) oscillation frequency and amplitude; (b) amplitude in the y -direction of the beam.

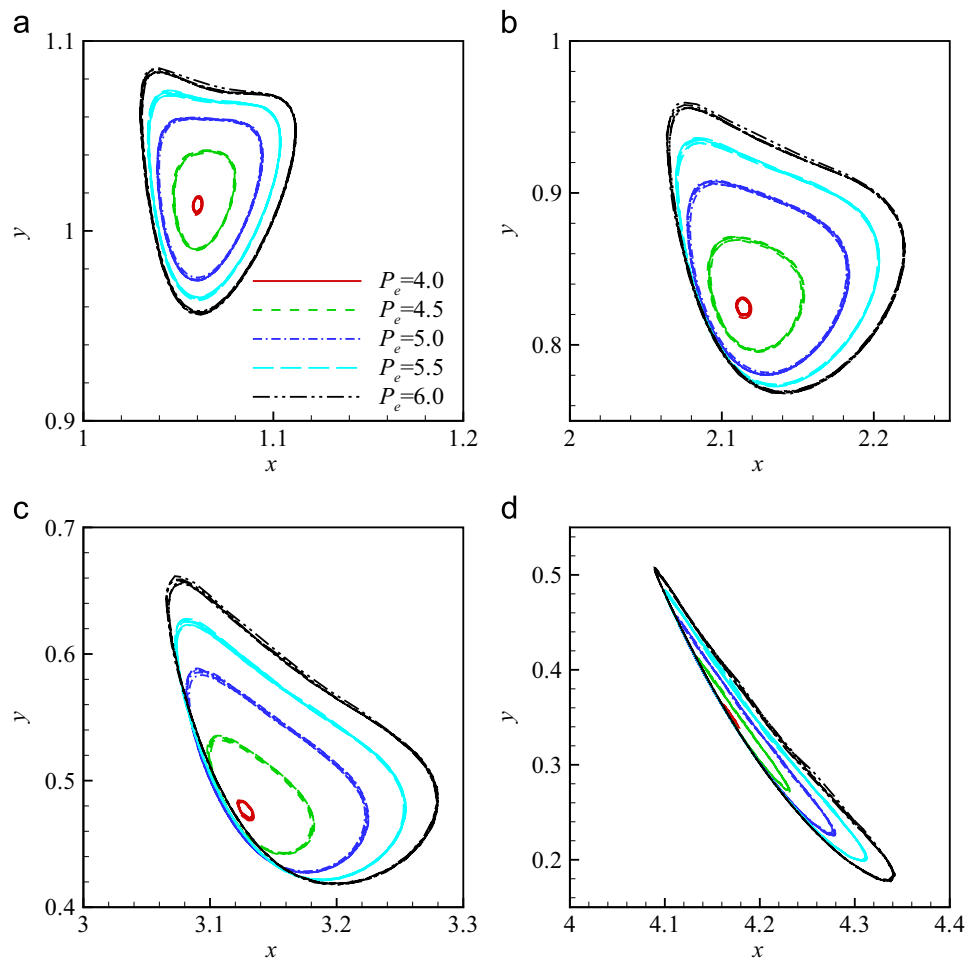


Fig. 3. The trajectories at points $x_0=1.0, 2.0, 3.0,$ and 4.0 on the beam for several values of P_e .

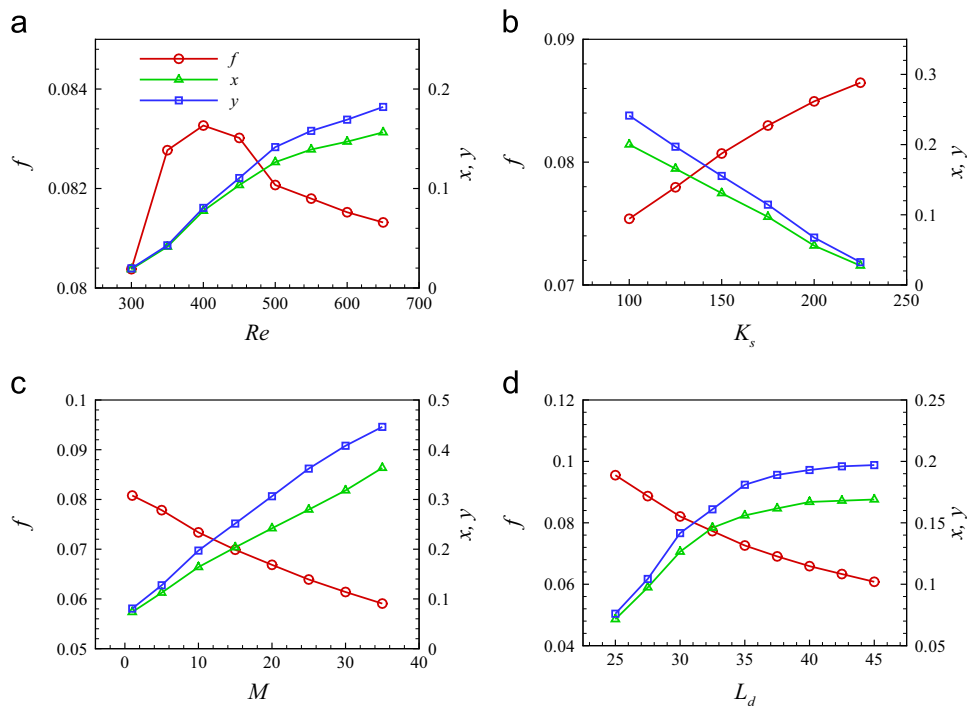


Fig. 4. Effects of some parameters on the oscillation frequency and amplitude: (a) the Reynolds number effect for $P_e=5.0$, $K_s=100$, and $M=1$; (b) the stretching stiffness effect for $Re=500$, $P_e=5.0$, and $M=10$; (c) the mass ratio effect for $Re=500$, $K_s=100$, and $P_e=4.5$; (d) the downstream length influence for $Re=500$, $K_s=100$, $M=1$, and $P_e=5.0$.

the beam is periodic. The greater the external pressure, the greater the area enclosed by the circumference of the closed trajectory. The trajectories at $x_0=1.0$ (upstream portion) are almost perpendicular to the main steam flow; those at $x_0=2.0$ and 3.0 (middle portion) are inclined towards the upstream of the flow; those of at $x_0=4.0$ (downstream portion) are so inclined and elongated by the flow to form a right-falling stroke. The oscillation amplitude at $x_0=4.0$ is the maximum among the four points.

The influence of the Reynolds number Re on the oscillation frequency and amplitude is analyzed. With fixed other parameters the Re ranges from 300 to 650 for the hemodynamics of the carotid artery. As shown in Fig. 4(a), the oscillation amplitudes in the x and y directions increase with Re . The maximum and minimum values of the oscillation frequency for those Reynolds numbers are not obvious with their difference less than 5%. Therefore, the Reynolds number has weak effect on the oscillation frequency for the range of Re .

Fig. 4(b) shows the effect of the stretching stiffness K_s on the oscillation frequency and amplitude. With the increase of K_s , the oscillation frequency increases slightly and the amplitude decreases almost linearly. Under a fixed external pressure P_e , a greater value of K_s corresponds to a harder elastic beam which undergoes smaller deformation, thus leading to less oscillation. This is similar to the effect of the decreased external P_e ; it means that increasing K_s and decreasing P_e have the similar effect on the oscillation amplitude of the beam. Our results indicate that veins are easier to collapse and undergo oscillation because in general veins are more flexible than the corresponding arteries.

The effect of the mass ratio M is further investigated. Usually, a greater value of M indicates that the inertia of the beam will have a greater impact in its oscillation. Fig. 4(c) shows that the amplitude increases and the frequency decreases with the increase of M , consistent with the previous work of a flapping filament in a viscous flow (Zhu and Peskin, 2002). These results together with those on the mass ratio suggest that once self-oscillation is excited

under similar circumstances, the degree of oscillation may become more severe in the arteries than in the veins because in general the arterial walls are thicker and the blood flow is faster in arteries.

Further we set L_u and L as constant by varying L_d to deal with the effect of the downstream length L_d . Fig. 4(d) shows the effect of the downstream length L_d on oscillation frequency and amplitude. It is seen that with the increase of L_d , the amplitude increases gradually and tends to constants. But the oscillation frequency decreases with the increase of L_d . These are caused by the resistance of downstream flow. Our results are essentially consistent with previous findings (Luo and Pedley, 1996; Wang et al., 2009).

These results obtained here provide both educational and clinical values to medical personnel who perform sphygmomanometry by an inflatable cuff or active compression on lower limbs' veins as a physical therapy for prevention of deep-vein thrombosis. It is important for them to be aware of the fact that the externally pressed veins may undergo collapse and self-excited oscillation which can be harmful to the vascular endothelial cells and smooth muscle cells particularly at the proximal ends of the veins.

Due to the oscillation of the elastic beam in the self-excited oscillation described above, the flow rate at the outlet is therefore time-dependent. Fig. 5(a) and (b) shows the time-dependent outlet flow rate Q for different values of P_e and M , respectively, where the rate Q is non-dimensionalized by the inlet one. It is obtained that a larger oscillation amplitude leads to a larger change in the flow rate at the outlet during one period of self-excited oscillation. The frequency of the flow rate change at the outlet is consistent with the frequency of the beam oscillation. These results imply that the self-excited oscillation of vessels may be harmful; it may hinder the in-time collection of oxygen-poor blood from veins into lungs and/or restrict the nutrient/oxygen supplied to the tissues downstream the arteries.

4.2. Pressure and wall shear stress along the beam

The oscillation frequency and amplitude of the beam have been investigated in the preceding section. We further study the shape of the oscillating beam and the pressure distribution along the beam during self-excited oscillation. As a typical case, Fig. 6(a) shows the y -coordinate of the lowest point during the self-excited oscillation and Fig. 6(b) demonstrates the shapes of the beam described on the x - y plane. The evolution of the beam shape is described for five instants marked in Fig. 6(a). In addition, it is identified that the oscillation of the beam is more intense under a larger P_e , indicating a larger amplitude during one period for any point on the beam.

Further, the corresponding pressure and wall shear stress (WSS) along the beam are shown in Fig. 6(c) and (d), respectively. The pressure remains nearly a constant on the upstream portion of the beam where the deformation is relatively small. The pressure drops significantly between $x=3.0$ and 4.0 before the lowest point of the beam. The pressure then increases slightly and remains

nearly a constant again on the remaining portion of the beam. The WSS gradually increases along the beam until $x=3.0$. After that the WSS undergoes a drastic spatial variation. It is elevated significantly reaching a peak, and then is lowered significantly reaching its minimum until near $x=4.5$ when it is slightly raised. Note that the drastic changes in the pressure and WSS take place on almost the same portion of the beam where the deformation is relatively large near the lowest point. Also among the several instants, the instant of the greatest deformation of the beam corresponds to the instant with the greatest peak in the WSS and greatest pressure difference between upstream and downstream portion of the beam. This rapid variation in the WSS and pressure can be damaging to endothelial cells lining the vascular intima and the smooth muscle cells consisting of the vascular media which can lead to the initialization of vascular diseases such as atherosclerosis and intimal hyperplasia (Ku, 1997). If the self-oscillation occurs on a vessel segment close to an atherosclerosis plaque, these significant spatial variations in the pressure and WSS can

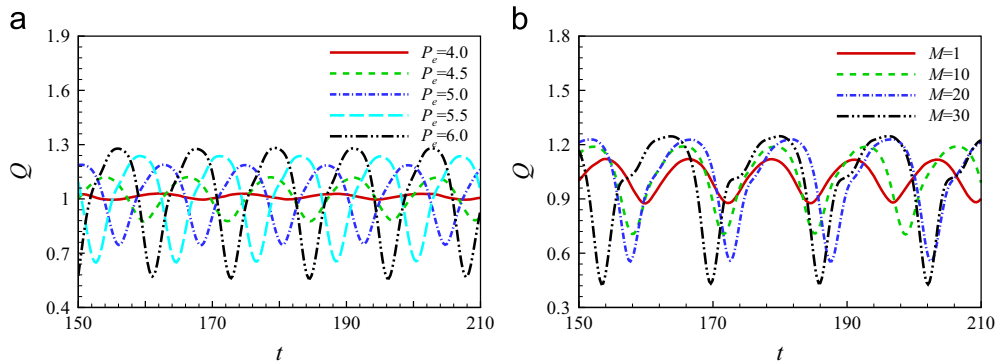


Fig. 5. The flow rate at the outlet: (a) for different external pressure P_e with $Re=500$, $K_s=100$, and $M=1$; (b) for different mass ratio M with $Re=500$, $K_s=100$, and $P_e=5.0$.

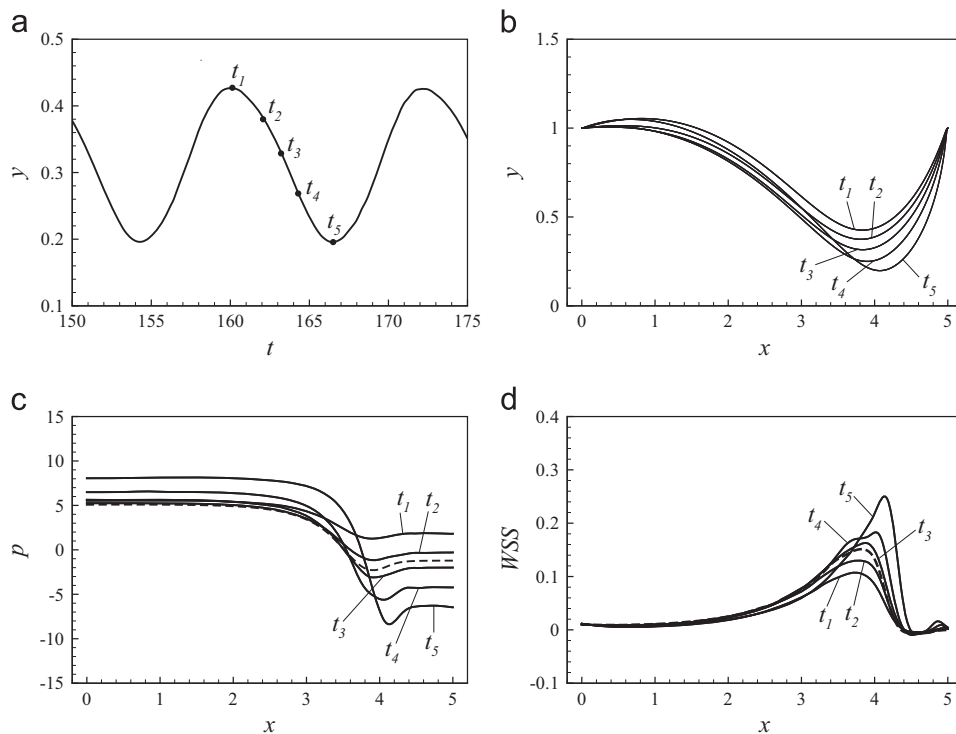


Fig. 6. (a) The y -coordinate of the lowest point for $K_s=100$, $M=1$, $Re=500$, and $P_e=5.0$; (b) the shapes corresponding to the five instants shown in (a); (c) and (d) the pressure and WSS along the beam for the five instants. The dashed lines in (c) and (d) represent the case with rigid boundary.

cause the rupture of the plaque and thus lead to heart attacks or strokes.

To demonstrate the flexibility effect of the beam, the beam shape and position at the middle instant of the five instants (i.e. the third instant) in Fig. 6(b) is used as the shape of a rigid beam. Then a simulation is also performed using the same dimensionless parameters as for the elastic beam. The pressure and WSS along the rigid beam are plotted in Fig. 6(c) and (d) as the dashed lines. Although the shape and position of the rigid beam are the same as those of the third instant, the corresponding pressure and WSS are different from the corresponding deformable beam. The curves of the pressure and WSS in the rigid case are all located between the corresponding two curves of the second and third instants of deformable case. Note that the flow states are unsteady in both the rigid and deformable cases.

Further, the energy exchange of the beam is investigated during self-excited oscillation. The total energy E_t of the beam contains the kinetic energy E_k and the elastic potential energy including the stretching energy E_{ps} and the bending energy E_{pb} . Fig. 7(a) shows the time history of energy in the beam. It is identified that the stretching energy of the beam is much greater than the kinetic energy and the bending energy. The majority of the total energy comes from the contribution of the stretching motion of the beam. The results indicate that it is reasonable to model healthy blood vessels as membranes only as used in the literatures (Pedley, 1992; Luo and Pedley, 1996), which significantly simplifies the numerical method and expedites the computation. However, the elastic

properties of diseased vessel, e.g. vessel with intimal hyperplasia, may be quite different, and both membrane and bending modes may be equally important.

Moreover, Fig. 7(b) shows the power of the external force acting on the beam. The external forces include the external pressure P_e and the force applied by fluid. For clear comparison, the total energy is also plotted. From the instant when the deformation and energy of the beam are both minimal, the energy of the beam increases and reach the maximum. During this process, P is always positive; it means that the external forces do positive work on the beam to increase its total energy. After that P becomes negative; it means that the external forces do negative work on the beam to decrease the total energy of the beam. At the same time, the deformation of the beam lessens and reaches the minimum again. Thus a period is complete and the next one begins.

4.3. Flow field and its evolution

To understand the flexibility effect on the flow structures, Figs. 8 and 9 show the instantaneous vorticity contours and streamlines for five instants which are marked in Fig. 6(a). In order to demonstrate the flexibility effect of the beam, the beam shape at the third instant is used as the shape of a corresponding rigid beam. The instantaneous vorticity contours and streamlines for the rigid case are also visualized in Fig. 10, in contrast with the third figure in Figs. 8 and 9. It is identified that in the deformable case, the region of shed vortices is closer to the downstream end of

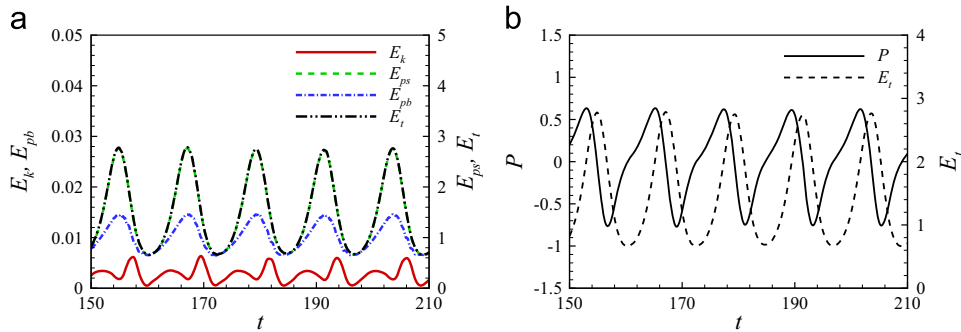


Fig. 7. (a) Time history of the beam energy with the set of parameters $Re=500$, $P_e=5.0$, $K_s=100$, and $M=1$; (b) the power of the external force acting on the beam and the total energy of the beam.

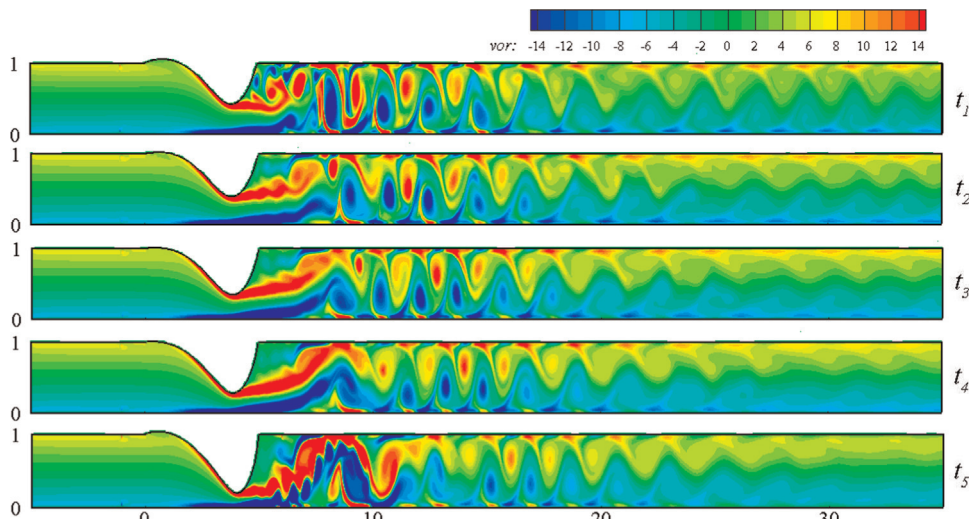


Fig. 8. The instantaneous vorticity contours for the five instants marked in Fig. 6(a) for the case with $K_s=100$, $M=1$, $Re=500$, and $P_e=5.0$.

the bulged wall, and large temporal variations in the pressure and WSS occur.

Similarly, another typical case for the dimensionless parameters $Re=300$, $P_e=4.5$, $K_s=100$, and $M=20$ is also investigated. The flow is steady in the rigid case, but is unsteady in the corresponding deformable case. The downstream flow behind the deformable beam is less violent and the vortex shedding is less intensive. Together these figures illustrate the obvious difference in the flow field and vortex shedding between the rigid and deformable boundaries.

Further, numerical investigation has been extensively used in modeling and simulation of blood flow in human blood vessels (Ku, 1997). However, almost all of the vessel models assume that the vessel walls are rigid, while the physiological vessel walls are deformable. To the best of our knowledge, there are not enough error analysis in the literature on the computed values of quantities such as the WSS and pressure compared to the actual physiological values (Perktold et al., 1994). Our results presented here, both qualitatively and quantitatively gauge on the errors caused by the rigid vessel wall assumption.

5. Summary

We have performed computational studies on a viscous incompressible flow past a 2D channel with part of its upper rigid wall being replaced by an elastic beam subject to external pressure on the outer surface. The flow is governed by the Navier–Stokes equations and numerically solved by the multi-block lattice Boltzmann method. The motion of the deformable beam is governed by the structural equation and solved by the finite difference method. The two-way mutual interaction of the fluid and the solid is handled by the momentum exchange method. After the method

and the code are rigorously verified and validated by existing results in the literature, a series of simulations are carried out on the effects of the parameters of the problem on the dynamics of this fluid-beam system including frequency, amplitude, and shape/trajectory of the self-excited oscillation of the elastic beam, pressure and WSS distributions on the inner surface of the beam. In addition, the qualitative and quantitative differences between rigid and elastic beams are illustrated by flow visualization in terms of vorticity contours and streamlines and by the pressure and WSS distributions. The flux at the outlet and the elastic potential energy of the beam are also investigated.

The results of our computational studies are summarized as follows. The self-excited oscillation of the deformable beam may be triggered by the externally applied pressure, and greater pressure results in stronger oscillation or greater amplitude. The lowest point of the beam during oscillation, i.e. the point of the beam with the greatest excursion along the y -axis, resides in towards the end portion of the beam. The stretching motion of the beam contributes most to the elastic potential energy of the beam. The bending mode of the beam is negligible in the oscillation fluid-beam system. As the stretching coefficient becomes greater or the beam is gradually stiffened, the oscillation amplitude decreases and the frequency increases. The greater the flow Reynolds number, the greater the oscillation amplitude, but the Reynolds number has very little effect on the frequency. The greater the mass ratio of the beam and fluid, the greater the oscillation amplitude, but the less the frequency. The pressure and WSS distributions along the beam undergo significant spatial variations near the same location where the beam reaches its lowest position. The obvious differences are observed for viscous flow past rigid and elastic beams in terms of vortex structures downstream and streamlines of the flow field, pressure and WSS distributions.

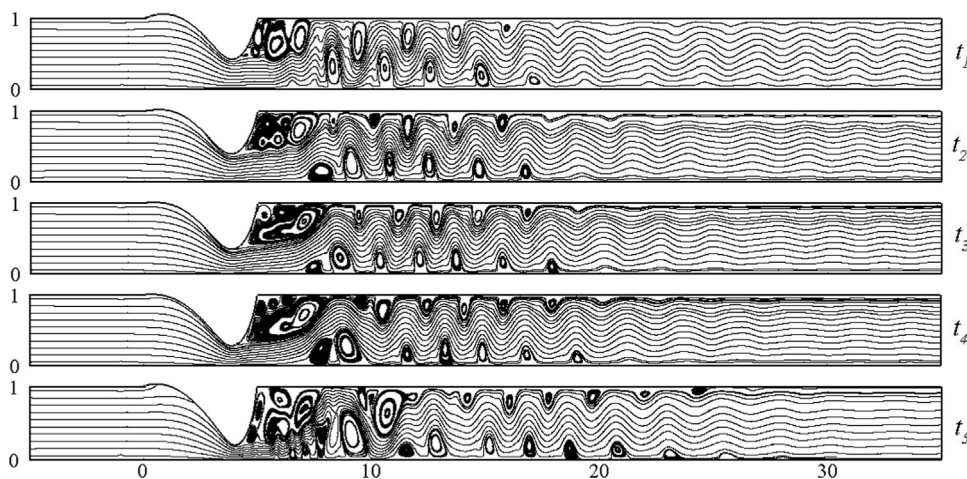


Fig. 9. The instantaneous streamlines for the five instants marked in Fig. 6(a) for the case with $K_s=100$, $M=1$, $Re=500$, and $P_e=5.0$.

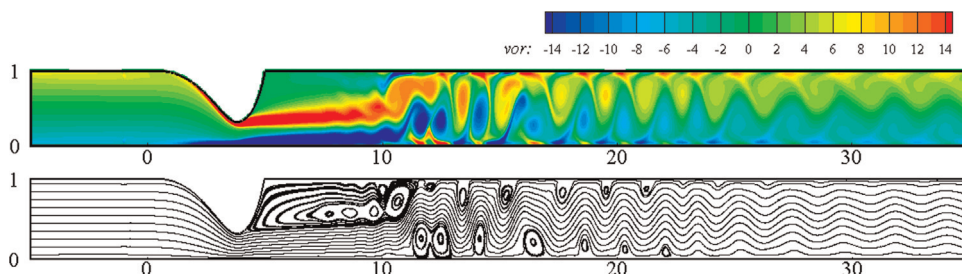


Fig. 10. The vorticity contours and streamlines for the case with rigid boundary.

Conflict of interest statement

None declared.

Acknowledgements

This work was supported by the National Science Foundation of China (Grant no. 11372304) and the 111 Project (Grant no. B07033). L. Zhu also would like to thank the support of the National Science Foundation of China (Grant no. 11172219).

References

- Bertram, C., 2008. Flow-induced oscillation of collapsed tubes and airway structures. *Respir. Physiol. Neurobiol.* 163, 256–265.
- Bertram, C., Raymond, C.J., Pedley, T.J., 1990. Mapping of instabilities for flow through collapsed tubes of differing length. *J. Fluids Struct.* 4, 125–153.
- Buxton, G., Clarke, N., 2006. Computational phlebology: the simulation of a vein valve. *J. Biol. Phys.* 32, 507–521.
- Cancelli, C., Pedley, T.J., 1985. A separated-flow model for collapsible-tube oscillations. *J. Fluid Mech.* 157, 375–404.
- Chen, S., Doolen, G., 1998. Lattice Boltzmann method for fluid flows. *Annu. Rev. Fluid Mech.* 30, 329–364.
- Dai, G., Gertler, J., Kamm, R., 1999. The effects of external compression on venous blood flow and tissue deformation in the lower leg. *J. Biomech. Eng.—Trans. ASME* 121, 557–564.
- Grotberg, J., Jensen, O., 2004. Biofluid mechanics in flexible tubes. *Annu. Rev. Fluid Mech.* 36, 121–147.
- Hazel, A., Heil, M., 2003. Steady finite-Reynolds-number flows in three-dimensional collapsible tubes. *J. Fluid Mech.* 486, 79–103.
- Heil, M., Boyle, J., 2010. Self-excited oscillations in three-dimensional collapsible tubes: simulating their onset and large-amplitude oscillations. *J. Fluid Mech.* 652, 405–426.
- Heil, M., Hazel, A., 2011. Fluid–structure interaction in internal physiological flows. *Annu. Rev. Fluid Mech.* 43, 141–162.
- Hua, R.N., Zhu, L., Lu, X.Y., 2013. Locomotion of a flapping flexible plate. *Phys. Fluids* 25, 121901.
- Hua, R.N., Zhu, L., Lu, X.Y., 2014. Dynamics of fluid flow over a circular flexible plate. *J. Fluid Mech.* 759, 56–72.
- Huang, W.X., Shin, S.J., Sung, H.J., 2007. Simulation of flexible filaments in a uniform flow by the immersed boundary method. *J. Comput. Phys.* 226, 2206–2228.
- Jensen, O.E., 1990. Instabilities of flow in a collapsed tube. *J. Fluid Mech.* 220, 623–659.
- Jensen, O.E., Heil, M.H., 2003. High-frequency self-excited oscillations in a collapsible-channel flow. *J. Fluid Mech.* 481, 235–268.
- Ku, D., 1997. Blood flow in arteries. *Annu. Rev. Fluid Mech.* 29, 399–434.
- Liu, H.F., Luo, X.Y., Cai, Z.X., Pedley, T.J., 2009. Sensitivity of unsteady collapsible channel flows to modelling assumptions. *Commun. Numer. Methods Eng.* 25, 483–504.
- Luo, X.Y., Pedley, T.J., 1996. A numerical simulation of unsteady flow in a two-dimensional collapsible channel. *J. Fluid Mech.* 314, 191–225.
- Luo, X.Y., Pedley, T.J., 1998. The effects of wall inertia on flow in a two-dimensional collapsible channel. *J. Fluid Mech.* 363, 253–280.
- Luo, X.Y., Cai, Z.X., Li, W.G., Pedley, T.J., 2008. The cascade structure of linear instability in collapsible channel flows. *J. Fluid Mech.* 600, 45–76.
- Marzo, A., Luo, X.Y., Bertram, C.D., 2005. Three-dimensional flow through a thick walled collapsible tube. *J. Fluids Struct.* 20, 817–835.
- Pedley, T.J., 1992. Longitudinal tension variation in collapsible channels: a new mechanism for the breakdown of steady flow. *ASME J. Biomech. Eng.* 114, 60–67.
- Perktold, K., Thurner, E., Kenner, T., 1994. Flow and stress characteristics in rigid walled and compliant carotid artery bifurcation models. *Med. Biol. Eng. Comput.* 32, 19–26.
- Tian, F.B., Luo, H., Zhu, L., Liao, J.C., Lu, X.Y., 2011a. An efficient immersed boundary-lattice Boltzmann method for the hydrodynamic interaction of elastic filaments. *J. Comput. Phys.* 230, 7266–7283.
- Tian, F.B., Luo, H., Zhu, L., Lu, X.Y., 2011b. Coupling modes of three filaments in side-by-side arrangement. *Phys. Fluids* 23, 111903.
- Wang, J., Chew, Y., Low, H., 2009. Effects of downstream system on self-excited oscillations in collapsible tubes. *Commun. Numer. Methods Eng.* 25, 429–445.
- Zhu, L., Peskin, C.S., 2002. Simulation of a flapping flexible filament in a flowing soap film by the immersed boundary method. *J. Comput. Phys.* 179, 452–468.